The Astrophysical Journal, 855:58 (10pp), 2018 March 1 https://doi.org/10.3847/1538-4357/aaac7c

Formation of Penumbra in a Sample of Active Regions Observed by the *SDO* Satellite

Mariarita Murabito[1], Francesca Zuccarello[1], Salvo L. Guglielmino[1], and Paolo Romano[2]
[1] Dipartimento di Fisica e Astronomia—Sezione Astrofisica, Università di Catania, Via S. Sofia 78, I-95125 Catania, Italy; mmurabito@oact.inaf.it
[2] INAF—Osservatorio Astrofisico di Catania, Via S. Sofia 78, I-95125 Catania, Italy
Received 2017 July 24; revised 2018 January 29; accepted 2018 January 29; published 2018 March 7

Abstract

Recently, high-resolution observations improved our understanding of the penumbra formation process around sunspots. In particular, two aspects have been carefully investigated: whether the settlement of the penumbra can occur between the main opposite magnetic polarities where new magnetic flux is still emerging, and the establishment of the Evershed flow. In this paper, we present the analysis of twelve active regions (ARs) where both the penumbra formation and the onset of the Evershed flow were observed. We used data acquired by the Helioseismic and Magnetic Imager (HMI) instrument on board the *Solar Dynamic Observatory* (*SDO*) satellite analyzing continuum images, magnetograms, and Dopplergrams of the selected ARs. The results obtained in our sample provided the following information about the stable settlement of the penumbra: eight spots formed the first stable penumbral sector in the region between the two opposite polarities, and nine spots formed on the opposite side. Moreover, eleven sunpots showed an inverse Evershed flow (i.e., a plasma motion directed toward the protospot border) before the penumbra formation, which changes within 1–6 hr into the classical Evershed flow as soon as the penumbra forms. Comparing our results with recent observations, we are able to discriminate between the different ways of penumbra formation. Moreover, we suggest that the change from inverse Evershed flow, visible before the penumbra appears, into the classical Evershed flow may be a signature of the formation of penumbral filaments.

Key words: Sun: magnetic fields – Sun: photosphere – sunspots

1. Introduction

The characteristics of solar active regions (ARs) are defined by the totality of observable phenomena from the photosphere to the corona as a result of the magnetic flux that has emerged from the convection zone (van Driel-Gesztelyi & Green 2015). The simplest ARs have a bipolar magnetic field configuration, but in general ARs may be built-up due to several bipoles emerging in close succession. In the photosphere, the most visible manifestations are sunspots, regions where magnetic field bundles are most concentrated, even if the magnetic field relevant to ARs is much more extended.

Recently, a number of studies have been carried out to better understand the sequence of processes at the base of the sunspot formation and, in particular, of the penumbra formation around protospots (Schlichenmaier et al. 2010; Rezaei et al. 2012; Shimizu et al. 2012; Romano et al. 2013, 2014). Although not specifically dealing with the process of the penumbra formation, Zwaan (1992) reported that the first penumbral sector of a sunspot forms toward the outer border of the AR, then sector by sector the penumbra encircles the umbra leaving a gap in the continuum intensity in the region facing the opposite polarity. Finally, when the emergence of the magnetic flux stops, the penumbra appears fulfilling the gap. On this subject, Schlichenmaier et al. (2010), studying AR NOAA 11024, found that the penumbra forms in sectors and generally on the side opposite to that between the two main opposite polarities. These authors noticed that, although individual filaments form on the side toward the opposite polarity, they are not stable and continuously appear and disappear, due to the ongoing flux emergence. For this reason they concluded that the penumbra cannot form in the region of flux emergence because this process prevents the settlement of the penumbral field. This seems in agreement with Zwaan (1992). In contrast, Murabito et al. (2017) reported on the formation of a stable penumbra on the side toward the opposite polarity in the following sunspot of the AR NOAA 11490. They noted in that area the presence of an arch filament system in the chromosphere and a filamentary pattern of the magnetic field similar to the sea-serpent configuration, as well as horizontal fields at the photospheric level before the formation of the penumbra. They explained the presence of horizontal fields owing to the changes in the inclination of overlying magnetic canopies between the two polarities. This hypothesis was supported by simulations of AR flux emergence carried out by MacTaggart et al. (2016).

Some authors (e.g., Leka & Skumanich 1998; Rezaei et al. 2012) estimated the critical value of some physical parameters above which penumbra formation takes place. They found that a magnetic flux threshold of (1–1.5) $\times$ 10^{20} Mx is needed for a penumbra to develop (Leka & Skumanich 1998). This threshold is in accordance with theoretical models (Rucklidge et al. 1995). In addition, Rezaei et al. (2012) found a critical value for the magnetic field strength, $B_{\rm crit} \lesssim 1.6$ kG, and a critical inclination angle of the magnetic field, $\gamma \gtrsim 60°$. The observations carried out by Jurčák et al. (2014) show evidence of a critical value of inclination at the protospot boundary. In particular, just at the onset of the penumbra, the field becomes more inclined. Later the umbra-penumbra (UP) boundary migrates inwards and the field on the boundary becomes more vertical.

In this context, according to Kitai et al. (2014) there are three ways to form the penumbra:

1. *Active accumulation of magnetic flux*: the magnetic flux concentrations move to form a denser magnetic concentration.

2. *Rapid emergence of magnetic fields*: new magnetic flux of the same polarity of the protospot emerges.
3. *Appearance of twisted or rotating magnetic flux tubes*: the penumbra filaments are seen rotating with respect to the radial direction from the umbra center.

In particular, they classified the AR 11024 studied by Schlichenmaier et al. (2010) and the AR 11490 studied by Romano et al. (2013, 2014) and Murabito et al. (2016, 2017) as cases of active accumulation of the magnetic flux.

Another aspect that has been investigated concerns the typical velocity pattern known as the Evershed flow (Evershed 1909). In recent observations, Schlichenmaier et al. (2012) and, in more detail, Murabito et al. (2016) found during the early stage of penumbra formation a line-of-sight (LOS) velocity pattern characterized by opposite sign (a so-called inverse Evershed flow), with respect to that observed later, when the penumbra has formed.

In this paper, in order to further investigate both aspects, i.e., whether penumbrae can form in the region between the main opposite sunspot polarities and the transition from inverse Evershed flow to the classical Evershed flow, we studied the penumbra formation of 12 ARs using observations carried out by the Helioseismic and Magnetic Imager (HMI; Scherrer et al. 2012) on board the *Solar Dynamic Observatory* (*SDO*; Scherrer et al. 2012) satellite. The paper is organized as follows: in the next section we describe the observations, presenting the results in Section 3. We summarize the main conclusions in Section 4.

2. Observations

We used the Space weather HMI AR Patches (SHARPs; Bobra et al. 2014) continuum filtegrams, LOS magnetograms, and Dopplergrams taken by HMI along the Fe I 617.3 nm line with a resolution of 1″ and a pixel size of 0.″5. To follow the evolution of the penumbra we used the HMI data with a cadence of 12 minutes.

We analyzed 12 ARs that appeared on the solar disk in 2011 and 2012, during the maximum of solar cycle 24. The ARs were chosen according to the following criteria:

1. penumbra formation occurring while the sunspots of the ARs were visible on the solar disk;
2. β-type magnetic field configuration during the entire passage of the AR over the visible solar hemisphere.

The latter requirement is chosen because the β-type magnetic field configuration is the simplest magnetic configuration, corresponding to a bipolar system, that allows the study of the preferential site of the penumbra formation.

In Table 1 the principal information about the sample of the ARs is listed. The second column provides the center position of the field of view (FOV) of the entire AR at the beginning of the observations (see Figures 1 and 2), and the third and fourth columns provide the time of the beginning and end of the observations. The end time indicates the time at which the formed stable penumbra completed its formation process.

To calibrate the Dopplergrams, we assumed that, on average, there is no plasma motion in the umbra (Rimmele 1994). Therefore, we defined the umbra with a threshold of the normalized continuum intensity, $I_c < 0.5$, calculated the mean velocity in the umbra, and subtracted it from the velocity in each pixel of the FOV. Being aware of the systematic errors associated with the *SDO* spacecraft orbital velocity (Couvidat et al. 2016), we compared this calibration with the standard HMI calibration and with that obtained by removing the 5 minute LOS velocity oscillations in the sunspot using a subsonic filter to highlight the peculiar signals of the flow associated with the penumbra formation. The velocities calibrated using the three different methods are comparable within an uncertainty of $\pm 100\ \mathrm{m\ s^{-1}}$. Taking into account this result, we report in the following the values of the velocity obtained by means of the first method described above.

Table 1
Selected ARs

AR	Position (arcsec)	Start Time (UT)	End Time (UT)
11150	(−610, −280)	2011 Jan 30 18:00	2011 Feb 02 17:48
11184	(−150, 375)	2011 Apr 03 06:00	2011 Apr 06 05:36
11210	(−200, 380)	2011 May 09 15:00	2011 May 11 05:24
11242	(100, 240)	2011 Jun 29 06:00	2011 Jul 01 05:48
11243	(−540, 230)	2012 Dec 09 00:00	2012 Dec 10 00:00
11466	(−600, 270)	2012 Apr 22 03:00	2012 Apr 22 23:00
11490[a]	(−180, −200)	2012 May 28 14:00	2012 May 29 21:00
11512	(750, −280)	2012 Jun 25 01:00	2012 Jun 28 00:00
11554	(−380, 150)	2012 Aug 24 06:00	2012 Aug 25 21:00
11610	(−520, −440)	2012 Nov 09 15:00	2012 Nov 11 06:00
11630	(−250, 310)	2012 Dec 09 00:00	2012 Dec 10 00:00
11640	(−410, 490)	2012 Dec 30 10:00	2013 Jan 03 10:00

Note.
[a] AR 11490 described and studied in Murabito et al. (2016, 2017).

3. Results

3.1. General Overview

Figures 1 and 2 display the continuum intensity (left column) and the simultaneous magnetograms (right column) of the selected ARs. All of the ARs follow the Hale's law (Hale & Nicholson 1925). In Table 2 we classified the protospots of the selected ARs as A or B depending on the side where the first stable penumbral sector forms, as represented in the cartoons shown in Figure 3. As a criterion to determine the stability of the penumbral filaments, we used a threshold of 10 times the granular life time, following the observations of Schlichenmaier et al. (2010). Then, we labeled the spots where the first stable penumbral sector forms away from the opposite polarity as A (see Figure 2, top panel). We indicated the spots where the penumbra starts to form between the two main polarities with B (see Figure 2, bottom panel). This information is listed in the third column of Table 2. The fourth column of Table 2 lists the time interval needed for the penumbra formation (in hours). We

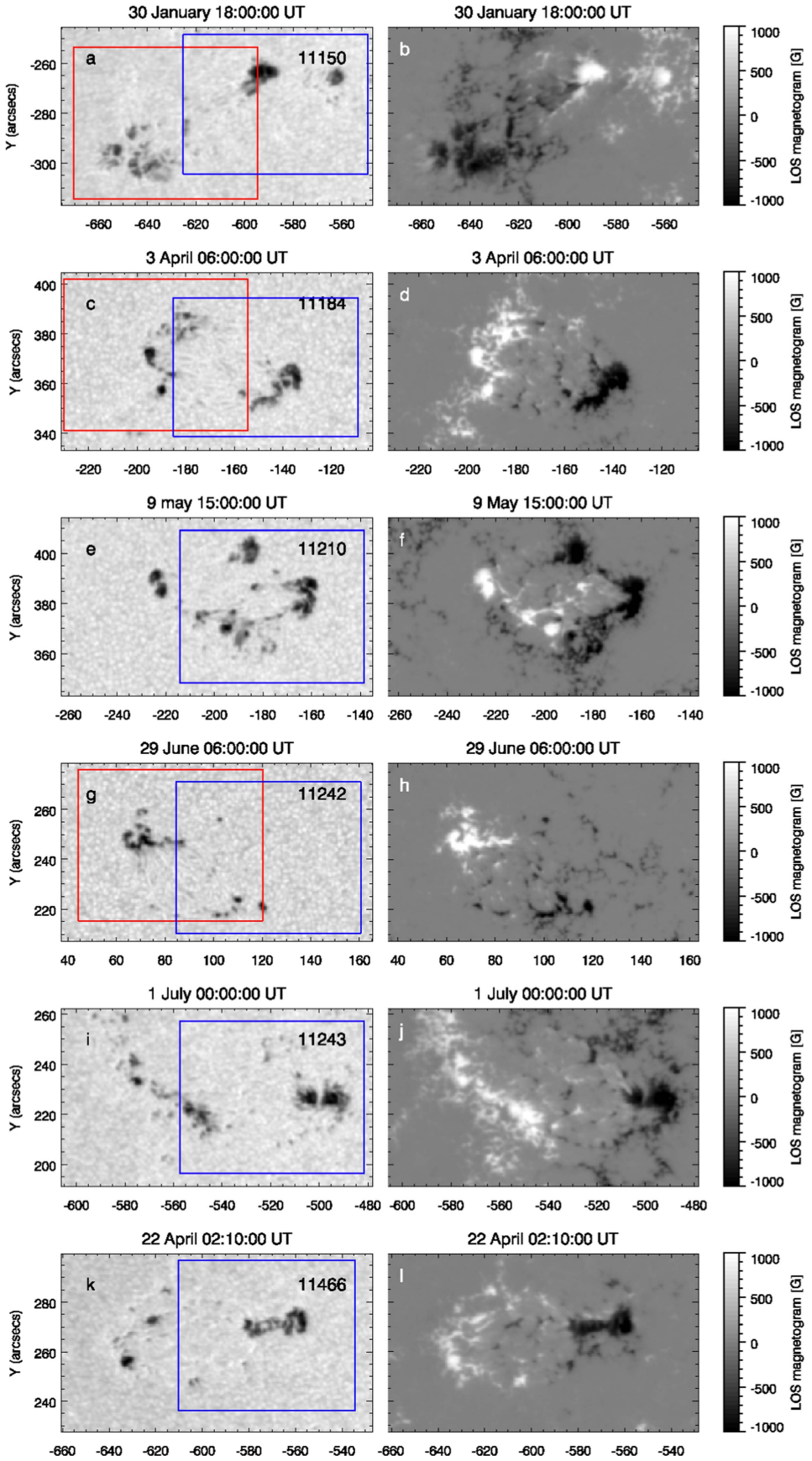

Figure 1. Continuum filtergrams (left column) and LOS magnetograms (right column) of six ARs of the sample at the beginning of the observation time. Here and in Figure 2 the red and blue boxes indicate the FOVs displayed in the Figures 4 and 5 for the following and preceding polarity of each AR, respectively. In all of the figures solar west is on the right and north is on the top.

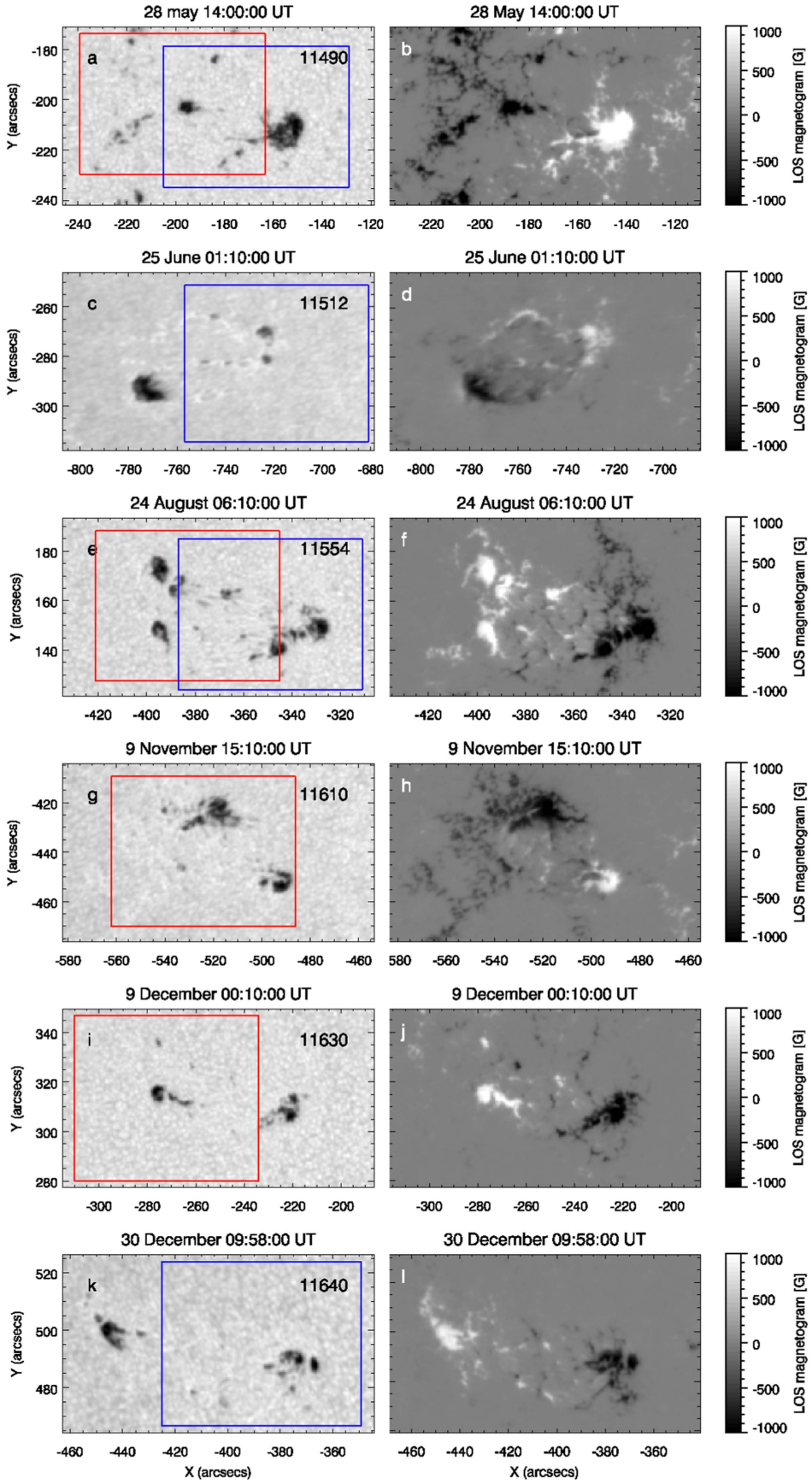

Figure 2. Continuum filtergrams (left column) and LOS magnetograms (rigth column) of the remaining six ARs of the sample at the beginning of the observation time.

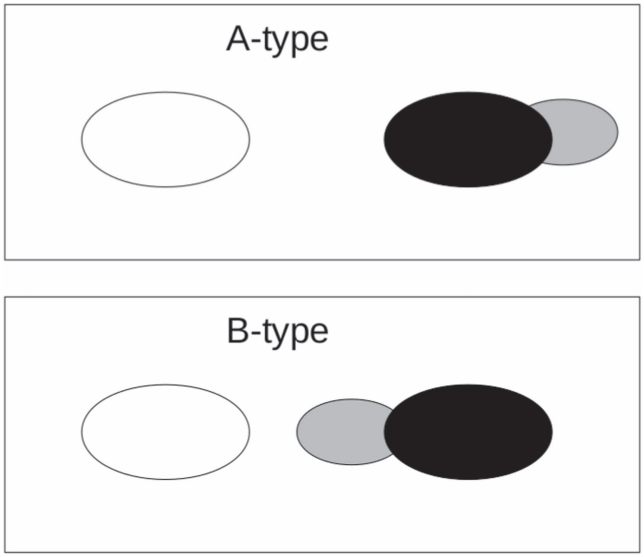

Figure 3. Representation of the criterion used to classify the penumbra formation for the selected ARs. The white and black ovals represent the following and preceding protospot, respectively. The gray oval represents the first penumbral sector.

Table 2
Properties of the Selected ARs

AR	Polarity[a]	Class[b]	Time (hr)	Penumbra Development[c]	Inverse Evershed Flow
NOAA	F	A	24	I	No
11150	**P**	B	26	I	Yes
NOAA	F	B	12	I	Yes
11184	P	A	71	C	Yes
NOAA					
11210	P	B	15	C	No
NOAA	F	B	38	C	No
11242	P	A	12	C	Yes
NOAA					
11243	P	A	77	C	Yes
NOAA					
11466	P	B	8	C	Yes
NOAA	F	B	27	C	No
11490[d]	P	A	24	C	Yes
NOAA					
11512	P	A	71	C	Yes
NOAA	F	A	8	I	No
11554	P	B	17	C	No
NOAA	**F**	B	24	C	Yes
11610					
NOAA	**F**	A	10	C	Yes
11630					
NOAA					
11640	**P**	A	55	C	Yes

Notes.
[a] P, preceding spot; F, following spot. Spots indicated with boldface are described in the main text.
[b] A, first penumbral sector forms away from the opposite polarity; B, first penumbral sector forms in the region between the two polarities.
[c] C, complete penumbra; I, penumbral sectors.
[d] Detailed analysis in Murabito et al. (2016, 2017).

reported in the fifth column whether the pore forms a complete penumbra, reaching the condition of a mature sunspot. Spots indicated with boldface (Table 2) are analyzed in detail in the following paragraphs, and the remaining ARs are shown in the Appendix in Figures 7–14. The missing spots have been excluded because the penumbra does not form or the first formation site is difficult to classify. We found that nine spots form the penumbra away from the opposite polarity (A-type) and eight spots form in the region facing the opposite polarity (B-type). The formation process in A-type spots has an average formation time of about 39 ± 29 hr. Conversely, the B-type spots form a penumbra faster, with an average formation time of about 21 ± 10 hr.

A-type: Figure 4 shows two clear examples of A-type spots: the following polarity of AR 11630 and the preceding polarity of AR 11640. In the AR 11630, the two polarities are well separated, as shown in the magnetogram acquired at 00:10 UT on December 9 (see Figure 2(j)). The continuum intensity map (Figure 2(i)) shows two dark structures with an elongated shape. Concerning the following polarity, the penumbra starts to form away from the opposite polarity (see the orange and the black arrows in Figures 4(b) and (a) that point to the area where the penumbra starts to form and to the opposite polarity region, respectively). Also, in Figures 4(a)–(d) we can see that the penumbral filaments to the northern and western side of the spot are inclined with respect to the radial direction from the umbra center. This is visible for about 8 hr, as can be seen in the yellow box of the continuum intensity maps of Figures 4 (a, c–d). This behavior can be ascribed to a peculiar penumbra formation process, where a twisting or rotating magnetic flux tube is crossing the photosphere. After about 22 hr from the beginning of the observations, the spot shows a full penumbra (see Figure 4(e)).

In the same way, the preceding polarity of AR 11640 shows the first penumbral filaments (see the orange arrow in Figure 4(g)) appearing on the side away from the opposite polarity (see the black arrow in Figure 4(f)) after 12 hr from the beginning of the observations. It shows a fully developed penumbra after 55 hr, i.e., at 4:10 UT on 2013 January 3, as shown in Figure 4(j). The penumbra formation process for this spot is the result of active accumulation of the magnetic flux.

B-type: Concerning B-type spots, one example is shown in Figures 5(a)–(e) for AR 11610. A small positive polarity and a more diffuse, negative polarity characterize this AR at 15:10 UT on November 11 (see Figures 1(g)–(h)). After about 2 hr from the beginning of the observations, the protospot in the negative polarity exhibits the first stable penumbral filaments on the side between the two polarities (see the orange and black arrows Figure 5(a), respectively). After 24 hr of active accumulation of the magnetic field, the penumbra surrounds the umbra, except in the area to the northwest (Figure 5(e)). In Figure 5(d) we can see that the penumbra on the side toward the opposite polarity appears earlier than on the side away from the opposite polarity.

Another example of a B-type spot is given by the preceding polarity of AR 11150. This AR is characterized by a diffuse negative polarity and a more compact positive polarity on January 30 at 18:00 UT (see Figures 1(a)–(b)). Initially, the preceding polarity consists of two positive pores. The biggest one, after 4 hr from the beginning of the observations, shows the first stable penumbral filaments in the area facing the opposite polarity (see the orange and black arrows in Figures 5(f) and (g), respectively). Noticeably, at the end of the penumbra formation process (Figure 5(j)), the penumbra covers only half of the umbra, the one facing the opposite polarity.

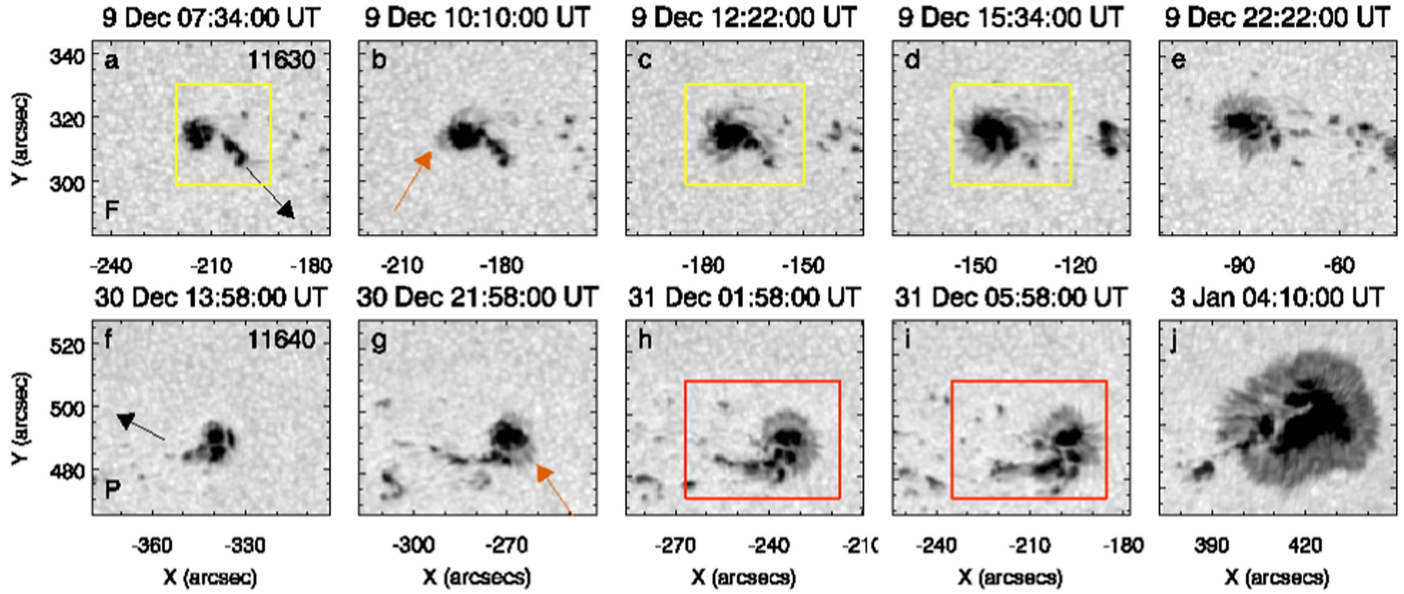

Figure 4. Evolution of the penumbra in the continuum maps of the following polarity of AR 11630 ((a)–(e)) and preceding polarity of AR 116400 ((f)–(j)). The colored boxes indicate two of the different ways of penumbra formation according to Kitai et al. (2014): appearance of twisted or rotating magnetic flux tubes (yellow) and active accumulation of magnetic fields (red), respectively. Here, in Figure 5, and in all of the figures in the Appendix, the black arrows point to the opposite polarity region.

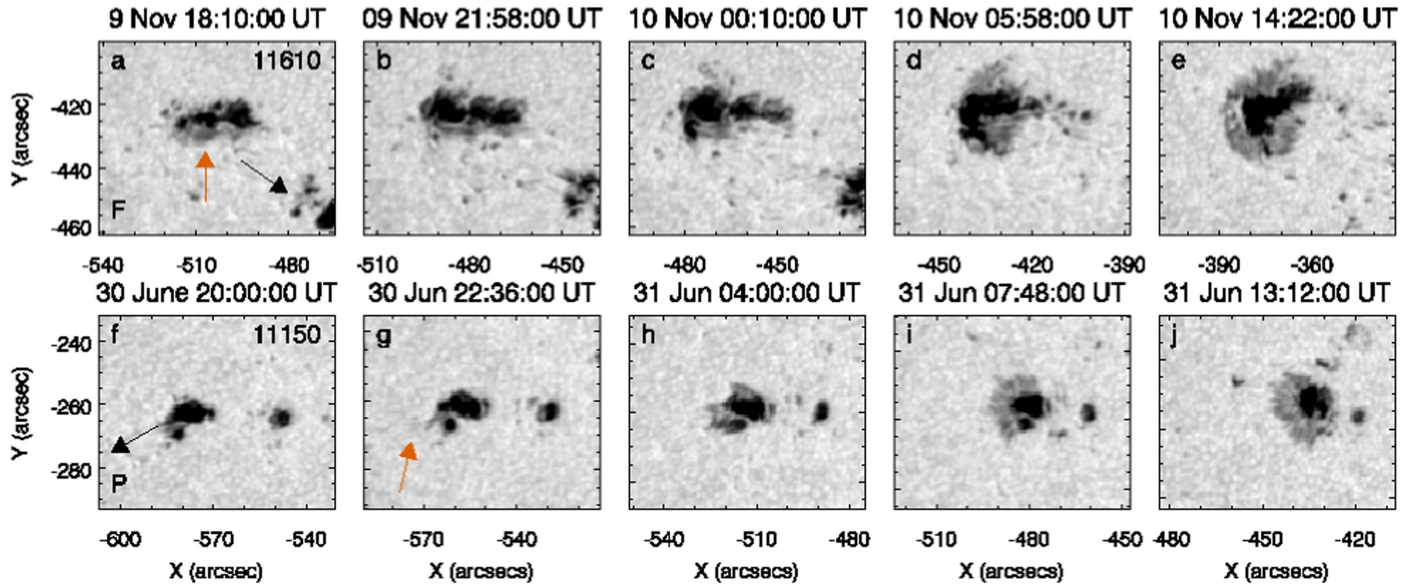

Figure 5. Same as in Figure 4 of the following polarity of AR 11610 ((a)–(e)) and the preceding polarity of AR 11150 ((f)–(j)).

3.2. Velocity Pattern

In Table 2 we report the presence of the inverse Evershed flow. In particular, in 11 spots we observe a flow of opposite sign with respect to that observed when the penumbra has formed, i.e., an inverse Evershed flow. In Figure 6, we show images of the continuum and LOS velocity maps for the following polarities of the AR 11610 and 11630, respectively. In these cases the inverse Evershed flow was clearly detected before the penumbra formation, although this process has already started.

Table 3 reports the mean values of the velocity before and after the penumbra formation, calculated inside the boxes shown in Figure 6.

In fact, in AR 11610, despite that the penumbra surrounds almost all of the umbra, there is a sector without penumbra on the eastern side of the following spot where we observe the onset of the Evershed flow in about 6 hr. The mean velocity before the onset of the Evershed flow is around $-160\ \mathrm{m\,s^{-1}}$, which becomes $210\ \mathrm{m\,s^{-1}}$ when the penumbra is completely formed. Concerning AR 11630 (Figure 6(i)–(p)), we observe at 11:00 UT (Figure 6(m)), when no penumbra filament is present (Figure 6(i)), that most of the area inside the black square is redshifted, with a mean velocity of about $220\ \mathrm{m\,s^{-1}}$. After 1 hr, filaments appear and the area becomes blueshifted (see Figures 6(j) and (n)).

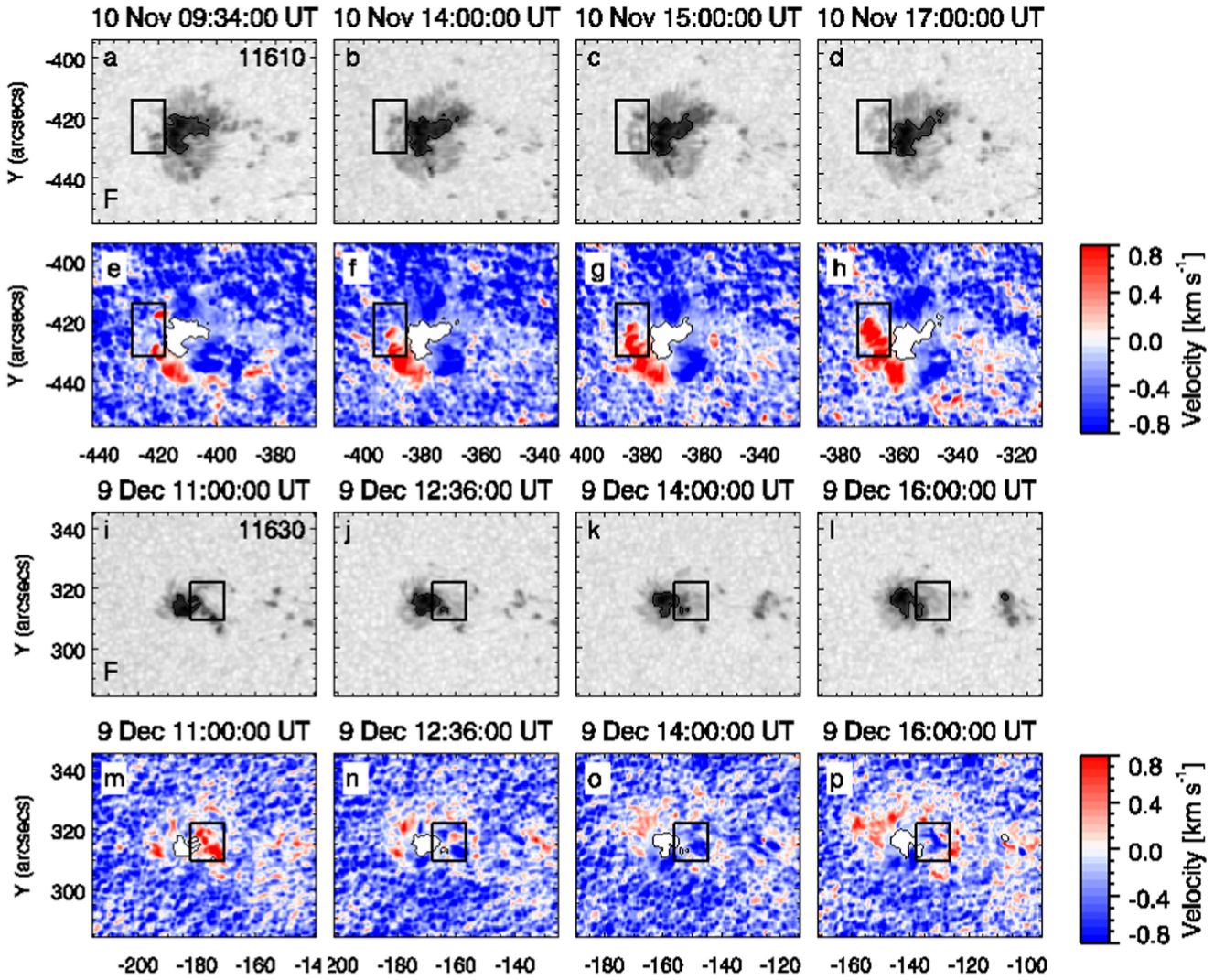

Figure 6. From top to bottom: zoom of the continuum and LOS velocity maps of the following sunspot of AR 11610 ((a)–(h)) and of the following sunspot of AR 11630 ((i)–(p)). The boxes in all of the panels indicate the regions where we calculated the values of the velocity reported in Table 3.

4. Discussion and Conclusions

In this paper we studied the penumbra formation in 12 ARs. We followed the evolution of the preceding and following spots using continuum and LOS velocity maps and, depending on where the first penumbral sector started to form, we classified the following and preceding polarities of each AR.

Despite the fact that not all of the spots in our sample are fully surrounded by a penumbra, we found that the last penumbral sector does not always appear on the side toward the opposite polarity (see the preceding polarity of AR 11150 in Figure 5), contrarily to what was reported by Zwaan (1992).

We found that in eight spots the first stable penumbral sector formed on the side toward the opposite polarity, and in nine spots it formed away from the opposite polarity (see Table 2).

We can also note that the time needed to form the penumbra seems to be related to the side where the penumbra appears. In particular, it seems that the penumbra formation in B-type spots is quicker (about 21 hr) than in the A-type spots (about 39 hr).

In addition, we highlight that, considering our sample, the penumbra formation is of an A–A type, i.e., according to Schlichenmaier et al. (2010) observations, or an A–B type, in agreement with the observations of Murabito et al. (2016, 2017).

Table 3
LOS Velocity around Sunspots

AR	Initial Velocity ($m\ s^{-1}$)	Final Velocity ($m\ s^{-1}$)
11610	−160	210
11630	220	−260

We also report observational evidence that the appearance of the penumbral filaments is correlated with the transition from the inverse Evershed flow. We found that the plasma velocity changes its sign even if we apply different calibration methods.

Unfortunately, the spatial resolution of HMI does not allow us to estimate the vertical component of the magnetic field to compare it with the critical value found by Jurcak (2011). The asymmetry of the observed penumbrae and the different locations where they can form suggest that the critical vertical magnetic field value found by Jurcak (2011) should be further investigated in order to find a condition that takes into account that the magnetic field could be not homogeneous along the UP boundary.

Our results can be compared with the recent sunspot simulations of Chen et al. (2017), where the evolution of emerging flux bundles generated in a solar convective dynamo is studied. Their preliminary results concerning the penumbral filaments and their formation indicate that the long penumbral filaments are more likely to appear in regions with ongoing flux emergence, on the side of the opposite polarity. The penumbral filaments found on the side away from the opposite polarity are fewer and shorter. Also in those simulations, the penumbral filaments are characterized by radial inflows, although part of the penumbra is dominated by an outflow in agreement with the observed Evershed effect. In our analysis, independently on the type and stage of the penumbra formation, i.e., if it concerns the formation of the first penumbral sector or the entire penumbra, we found that the absence of penumbral filaments in the continuum intensity is associated to an inverse Evershed flow that changes its sign when the penumbra appears in about 1–6 hr. This confirms the scenario proposed by Murabito et al. (2016) for the onset of the classical Evershed flow. Thus, these systematic changes of direction of the plasma flows around the pore appear to be a signature of the formation of stable penumbral filaments.

Finally, according to the findings of Kitai et al. (2014), we confirm that there are different paths for the penumbra formation. In our study, in fact, we found evidence of some paths proposed by Kitai et al. (2014): active accumulation of the magnetic field and appearance of a twisted and rotating magnetic flux tube. Moreover, they found these formation paths in a single $\beta-\gamma$ AR. Our sample is composed only by β AR, and we noted that not all of the formation paths are included in the formation relevant to a single AR.

These clues could be investigated in more detail benefiting from the extremely high resolution of the next generation of solar telescopes such as the GREGOR telescope (Schmidt et al. 2012), the Daniel K. Inouye Solar Telescope (DKIST, formerly the Advanced Technology Solar Telescope (ATST); Keil et al. 2010), and the European Solar Telescope (EST; Collados et al. 2010).

This work was supported by the Istituto Nazionale di Astrofisica (PRIN-INAF-2014), the University of Catania (PRIN MIUR 2012), and from the European Union's Horizon 2020 research and innovation program under grant agreement No 739500.

Appendix

Figures 7–14 display the continuum maps relevant to the evolution of the ARs analyzed in Table 2, which are not described in the main text.

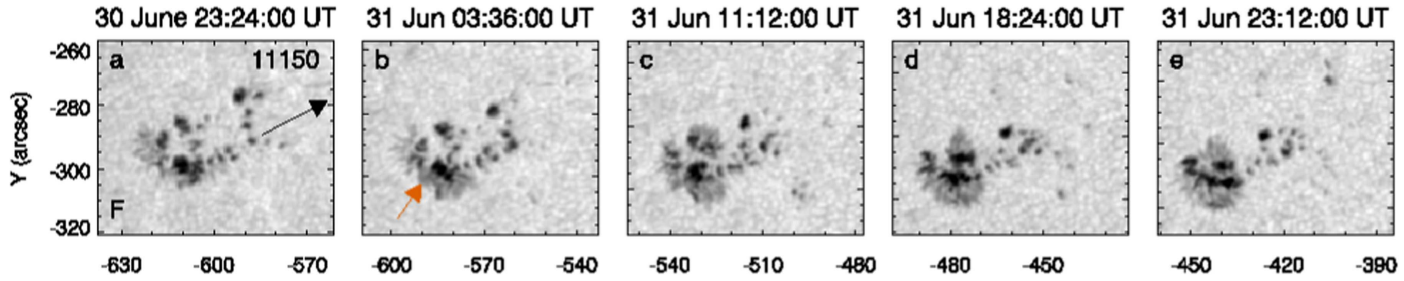

Figure 7. Same as Figure 4 for the following polarity of AR 11150

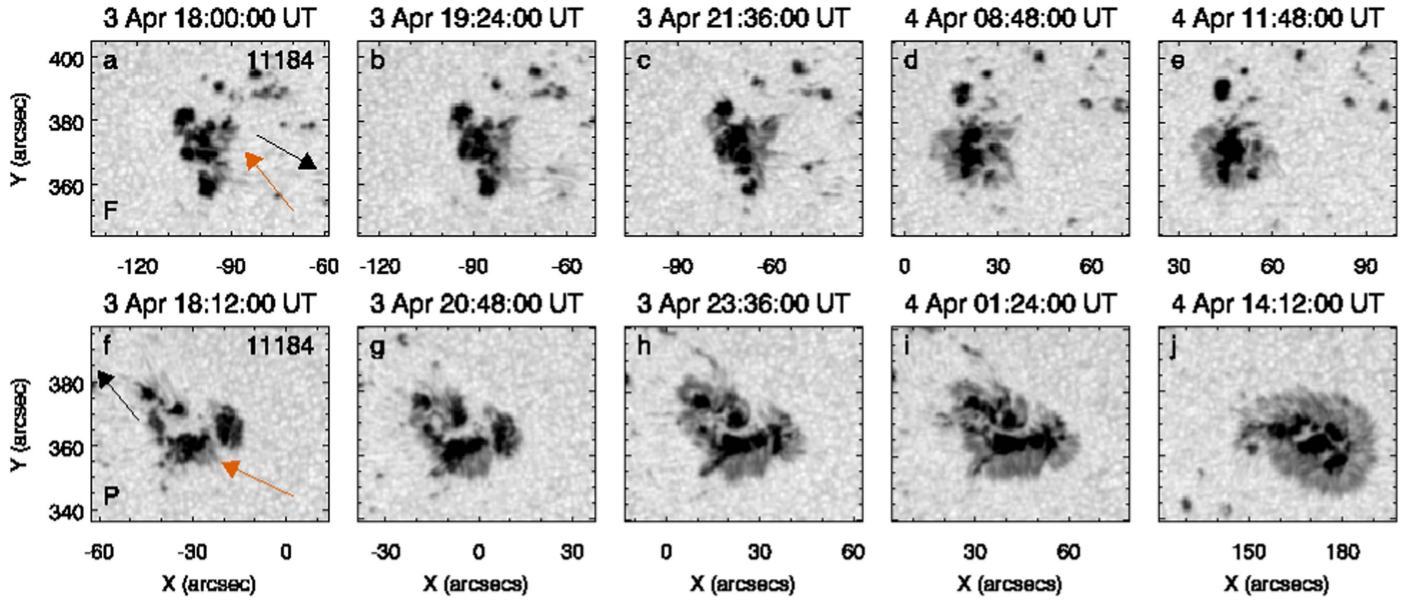

Figure 8. Same in Figure 4, for AR 11184.

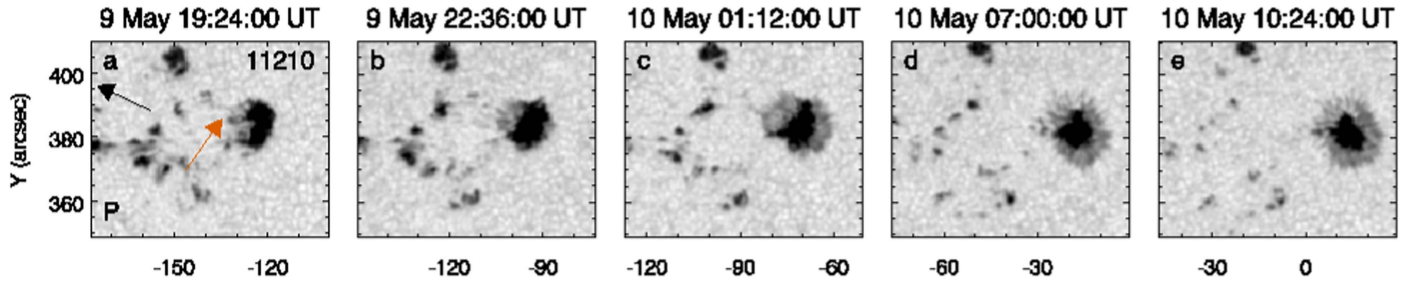

Figure 9. Same in Figure 4, for the preceding polarity of AR 11210.

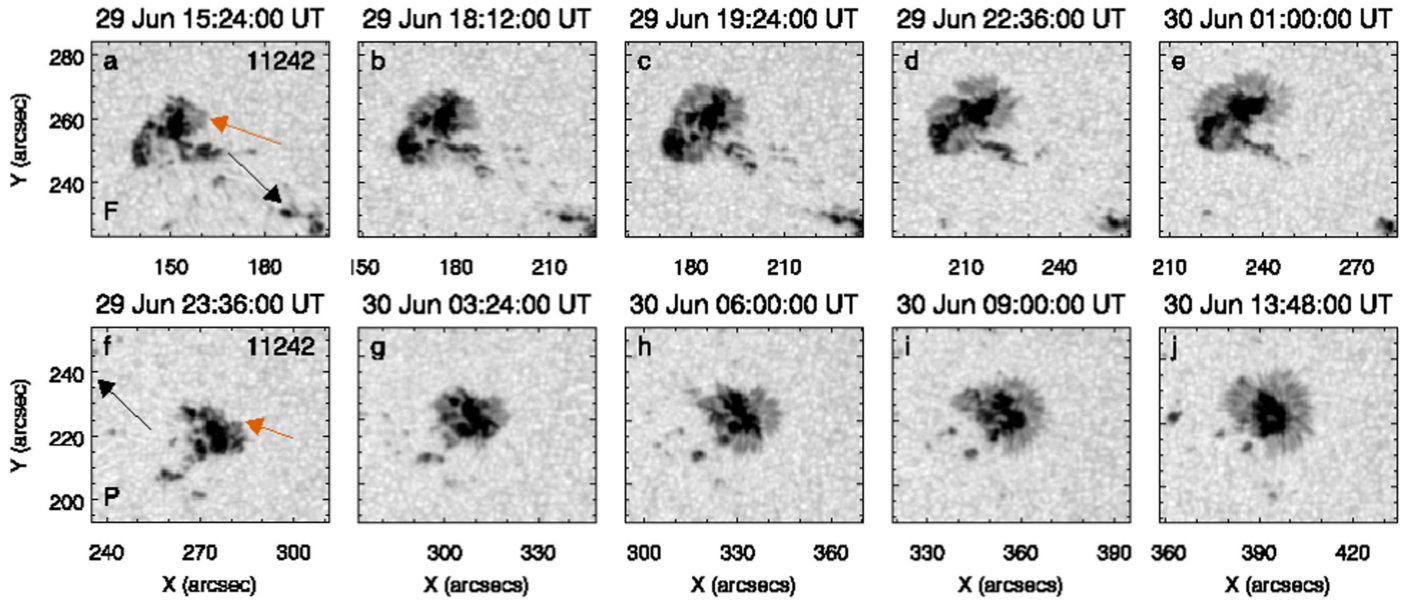

Figure 10. Same in Figure 4, for AR 11242.

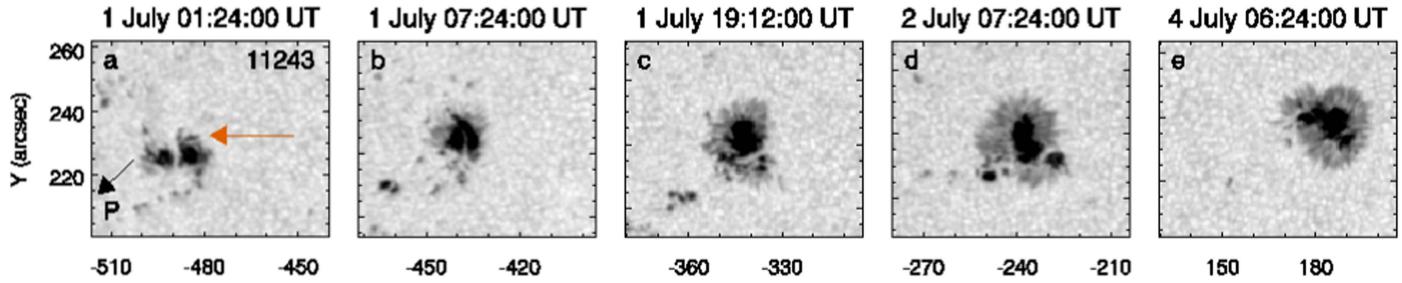

Figure 11. Same in Figure 4, for the preceding polarity of AR 11243.

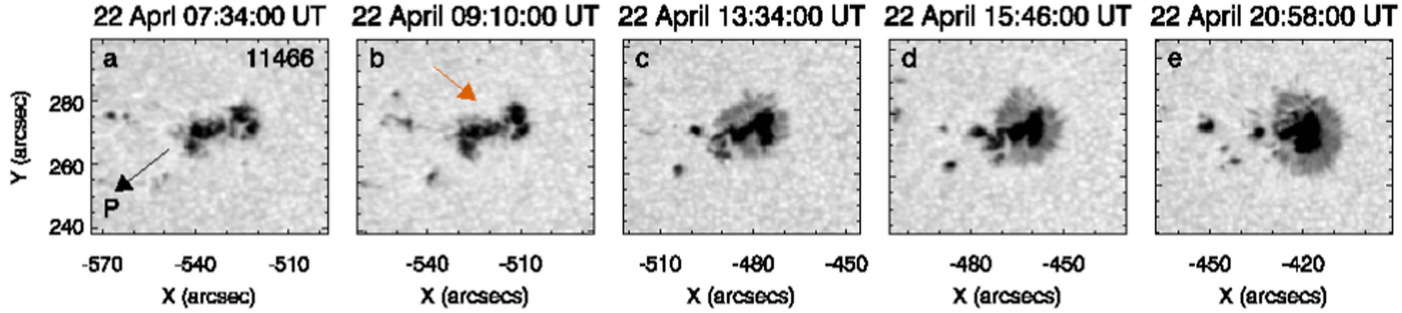

Figure 12. Same in Figure 4, for the preceding polarity of AR 11466.

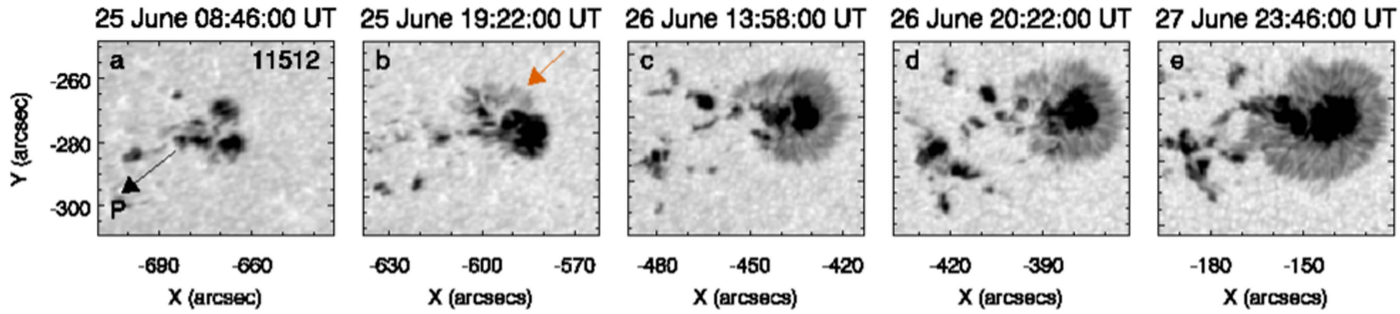

Figure 13. Same in Figure 4, for the preceding polarity of AR 11512.

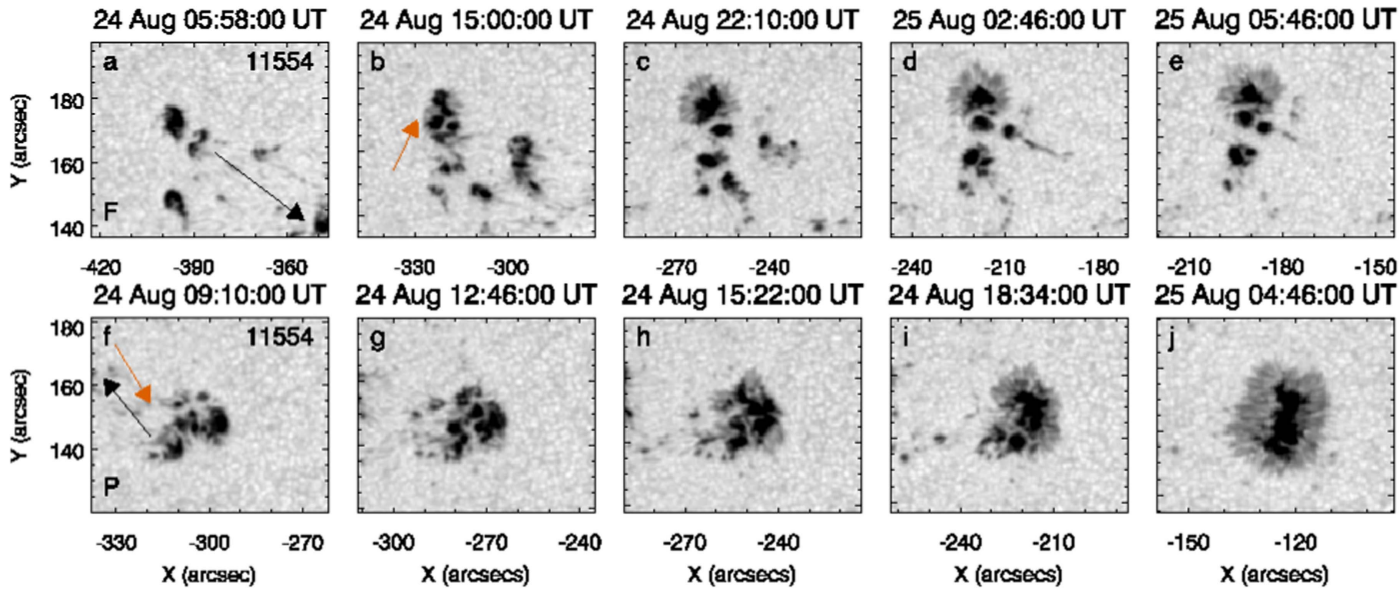

Figure 14. Same as in Figure 4, for AR 11554.

ORCID iDs

Mariarita Murabito https://orcid.org/0000-0002-0144-2252
Francesca Zuccarello https://orcid.org/0000-0003-1853-2550
Salvo L. Guglielmino https://orcid.org/0000-0002-1837-2262
Paolo Romano https://orcid.org/0000-0001-7066-6674

References

Bobra, M. G., Sun, X., Hoeksema, J. T., et al. 2014, SoPh, 289, 3549
Chen, F., Rempel, M., & Fan, Y. 2017, ApJ, 846, 149
Cheung, M. C. M., Schüssler, M., & Moreno-Insertis, F. 2007, A&A, 467, 703
Collados, M., Bettonvil, F., Cavaller, L. & EST Team 2010, AN, 331, 615
Couvidat, S., Schou, J., Hoeksema, J. T., et al. 2016, SoPh, 291, 1887
Evershed, J. 1909, Obs, 32, 291
Fan, Y. 2009, LRSP, 6, 4
Hale, G. E., & Nicholson, S. B. 1925, ApJ, 62, 270
Jurcak, J. 2011, A&A, 531, A118
Jurcak, J., Bello González, N., Schlichenmaier, R., & Rezaei, R. 2011, A&A, 580, L1
Jurčák, J., Bello González, N., Schlichenmaier, R., & Rezaei, R. 2014, PASJ, 66, S3
Keil, S. L., Rimmele, T. R., Wagner, J. & ATST Team 2010, AN, 331, 609
Kitai, R., Watanabe, H., & Otsuji, K. 2014, PASJ, 66, S11
Leka, K. D., & Skumanich, A. 1998, ApJ, 507, 454
MacTaggart, D., Guglielmino, S. L., & Zuccarello, F. 2016, ApJL, 831, L4
Martínez-Sykora, J., Hansteen, V., & Carlsson, M. 2008, ApJ, 679, 871
Murabito, M., Romano, P., Guglielmino, S. L., & Zuccarello, F. 2017, ApJ, 834, 76
Murabito, M., Romano, P., Guglielmino, S. L., Zuccarello, F., & Solanki, S. K. 2016, ApJ, 825, 75
Rezaei, R., Bello González, N., & Schlichenmaier, R. 2012, A&A, 537, A19
Rimmele, T. R. 1994, A&A, 290, 972
Romano, P., Frasca, D., Guglielmino, S. L., et al. 2013, ApJL, 771, L3
Romano, P., Guglielmino, S. L., Cristaldi, A., et al. 2014, ApJ, 784, A10
Rucklidge, A. M., Schmidt, H. U., & Weiss, N. O. 1995, MNRAS, 273, 491
Scherrer, P. H., Schou, J., Bush, R. I., et al. 2012, SoPh, 275, 207
Schlichenmaier, R., Rezaei, R., & Bello González, N. 2012, in ASP Conf. Ser. 455, IV Hinode Science Meeting: Unsolved Problems and Recent Insights, ed. L. Bellot Rubio, F. Reale, & M. Carlsson (San Francisco, CA: ASP), 61
Schlichenmaier, R., Rezaei, R., Bello González, N., & Waldmann, T. A. 2010, A&A, 512, L1
Schmidt, W., von der Luhe, O., Volkmer, R., et al. 2012, AN, 333, 796
Shimizu, T., Ichimoto, K., & Suematsu, Y. 2012, ApJL, 747, L18
van Driel-Gesztelyi, L., & Green, L. M. 2015, LRSP, 12, 1
Zwaan, C. 1992, in Proc. NATO Advanced Research Workshop, Sunspots: Theory and Observations (NATO ASI Series C375), ed. J. H. Thomas & N. O. Weiss (Dordrecht: Kluwer), 75